ADVANCED FUNCTIONAL MATERIALS
www.afm-journal.de

Greener Electrochemical Synthesis of High Quality Graphene Nanosheets Directly from Pencil and its SPR Sensing Application

Virendra V. Singh, Garima Gupta, Anirudh Batra, Anil K. Nigam, Mannan Boopathi, Pranav K. Gutch, Brajesh K. Tripathi, Anchal Srivastava, Merwyn Samuel, Gauri S. Agarwal, Beer Singh, and Rajagopalan Vijayaraghavan*

A green, simple, and cost effective electrochemical method to synthesize pure graphene oxide (GO) and graphene nanosheets (GNs) using pencil in ionic liquid medium is reported. The morphology and microstructure of prepared GNs and GO are examined using scanning electron microscopy (SEM), transmission electron microscopy (TEM), atomic force microscopy (AFM), X-ray diffraction (XRD), and Raman spectroscopy; the experiments confirm the formation of high quality graphene. The synthesized GO is used for the real-time and label-free surface plasmon resonance (SPR) sensing of the biological warfare agent *Salmonella typhi*.

1. Introduction

Graphene is a single layer graphite and has attracted intense scientific interest in recent years because of its 2D structure and unique physical properties, such as high intrinsic carrier mobility at room temperature, excellent mechanical strength, and electrical and thermal conductivity, which are comparable to the in-plane value of graphite.[1,2] Because of the unique properties and potential applications of graphene in nanoelectronics, energy storage materials, polymer composite materials, catalysis, drug delivery, and sensing, the approaches for the preparation of high-quality graphene on a large-scale were intensively explored in recent years.[3] Graphene was originally isolated through micromechanical cleavage of graphite; this discovery was recently honored with the Nobel Prize in physics in 2010.[4] However, limitations on this micromechanical cleavage method are the lack of scalability and smaller size graphene flakes.[5] Current methods for preparation of graphene nanosheets (GNs) include chemical vapor deposition (CVD),[6] ultrasonication-assisted exfoliation of graphite,[7] epitaxial growth on electrically insulating surface,[8] and solution-based chemical reduction of graphene oxide (GO).[9] Graphene obtained by the above first three methods showed limited uniformity or unsuitable single layer selectivity.[10] Moreover, the low productivity, non-viability for commercialization, time consuming nature, and use of high temperature makes the above three methods unsuitable for large-scale production of graphene.[11] In view of the above, chemical exfoliation of graphite to GO by the Hummers method (oxidation of graphite into thin GO) and then GO to graphene by chemical or thermal reduction received much attention due to low-cost requirements and mass production capability.[12–15] However, most of the reported chemical methods use harsh oxidizers, such as $H_2SO_4/KMnO_4$ or carboxylic acid, formic acid, and an excess of organic solvents for subsequent exfoliation, and these are all environmentally detrimental.[16–18] In addition, the subsequent reduction of GO sheets to graphene typically requires a chemical reductant such as hydrazine or sodium borohydride and high temperature heating in order to recover the graphitic structure.[19] Moreover, the severe poisonous and explosive characteristics of hydrazine or sodium borohydride and its derivates require precautions when large quantities are used and this makes the process difficult in actual conditions.[20] A few environmentally friendly processes are available[21,22] to reduce GO to graphene either by chemical or electrochemical methods, however, a unified 'green' approach in a one pot synthesis of graphene has not been reported so far.

Ionic liquids (ILs) are a class of new materials and have attracted many scientists for green chemistry applications due to their specific properties that include high ionic conductivity, nonvolatility, low vapor pressure, and high chemical and thermal stability.[23] This new chemical group can reduce the use of hazardous and polluting organic solvents in various new syntheses due to their unique characteristics. ILs are extensively used as a reaction medium for the synthesis of conducting polymers and nanoparticles[24–27] due to their entire ionic composition, intrinsic conductivity, negligible vapor pressure, and wide

Dr. V. V. Singh, G. Gupta, A. K. Nigam,
Dr. M. Boopathi, Dr. P. K. Gutch, B. K. Tripathi,
A. Srivastava, M. Samuel, Dr. G. S. Agarwal,
Dr. B. Singh, Dr. R. Vijayaraghavan
Defence Research and Development Establishment
DRDO, Gwalior-474002, India
E-mail: boopathi@drde.drdo.in
A. Batra
Amity University
Noida-201303, India

DOI: 10.1002/adfm.201102525

electrochemical potential window. Keeping all these properties of ILs in mind, we have explored and used IL for the synthesis of GNs.

Here, we report a greener and novel electrochemical approach towards ecofriendly synthesis of GNs and GO by using pencil. Moreover, our process has several advantages such as simplicity, high productivity, economical viability, one pot synthesis, and short processing time when compared to previously reported techniques and methods. In addition, this novel electrochemical method does not generate toxic gases during the exfoliation as generated in other wet chemical methods and it can be performed under normal conditions at room temperature. To the best of our knowledge, there is so far no report of a greener, one-pot electrochemical synthesis of GNs in neat IL. Moreover, we have utilized the synthesized GO to develop a real-time and label-free surface plasmon resonance (SPR) optical method for the sensing of biological warfare agent (BWA) *Salmonella typhi* monoclonal antibody (*S. typhi* Mab) by modifying the SPR gold chip with GO and *Salmonella typhi antigen* (*S. typhi* Ag). *S. typhi* is a genus of gram-negative, facultative anaerobic, non-spore-forming, and rod-shaped bacteria. *Salmonella* serotype *typhi* is human specific, and causes enteric (typhoid) fever in humans.[28] *Salmonella* contamination of food can cause large economic losses and, more crucially, it is a threat to public health; however, the detection of *Salmonella* bacteria remains a challenging and potential issue for food safety and security.[29] Various methods such as enzyme-linked immunosorbent assay (ELISA),[30] multiplex polymerase chain reaction (PCR),[31,32] and Widal agglutination test[33] were developed for the detection of *S. typhi*. All these developed methods require the labeling of antibodies, precipitation of antigen antibody complexes, proteins in purified conditions, etc. and the sensitivity of the assay for the detection of antigen antibody interactions are very low. SPR sensors offer several advantages over other detection methods including continuous real-time monitoring of biomolecular interactions. Direct detection with SPR sensors does not continuously consume reagents, as do the majority of other detection procedures based on ELISA. To the best of our knowledge, no report is available to date in the literature for the sensing of BWA *S. typhi* Mab using SPR and, also to the best of our knowledge, this is the first report about the utilization of GO-modified SPR gold chips for sensing purposes. Hence, the present work was undertaken based on our earlier SPR sensing studies.[34,35] Moreover, the experimental parameters that affect the SPR angle change such as temperature and pH were also varied and optimized.

2. Results and Discussion

In the electrochemical synthesis of GNs, a conventional three-electrode system was used, consisting of pencil as the working electrode, platinum (Pt) as a quasi reference electrode, and Pt spiral as counter electrode in 10 mL of triethyl sulfonium bis(trifluoromethyl sulfonyl) imide medium. **Scheme 1** illustrates the experimental setup, where pencil was employed as working electrode to get GNs during electrochemical exfoliation. In this study, a static potential of 0 V was applied to the pencil for a period of 120 s, followed by ramping the bias to +8 V for 600 s and then again stepped back to –8 V for another 600 s under normal conditions at room temperature. The initial 0 V helps to wet the sample and causes gentle intercalation of IL to the grain boundary of pencil.[36,37] The pencil remained as single piece until applying a high bias of +8 V/–8 V. After the completion of the experiment, a black precipitate of GNs was obtained at the bottom of the electrochemical vessel. The GO was also obtained by applying a static potential of 0 V to the pencil for a period of 120 s, followed by ramping the bias to +8 V for 600 s at room temperature, then this graphite oxide was thoroughly washed and filtered by Milli-Q water followed by dialysis of sample for three days in order to remove intercalating species if any present in the sample. The graphite oxide was suspended in a mixture of ethanol and water and exfoliated through ultrasonication for 1 h in order to get the GO.[38]

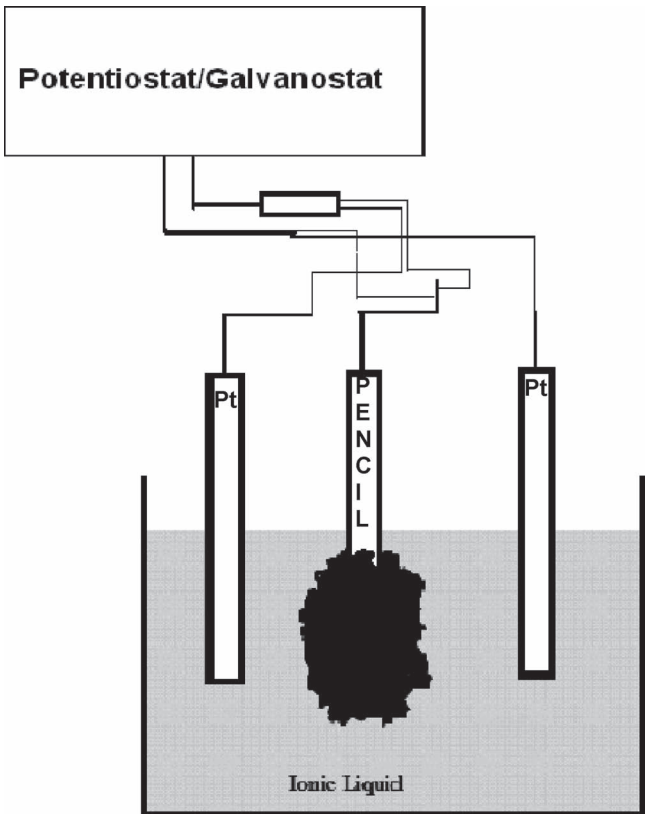

Scheme 1. Experimental set-up diagram showing the exfoliation of the pencil.

Moreover, we have also optimized and compared the bias potential and found that electrochemical exfoliation of pencil was maximum at +8 V/–8 V, as the whole exfoliation process can be finished in a few minutes (Table S1, Supporting information). It is noteworthy to mention that the previously reported methods for the electrochemical exfoliation of graphite require more time and an excess use of organic solvents, which is environmentally detrimental.The GNs obtained in this study are further characterized.

The thermal behaviors of the pencil, GO, and GNs were investigated by thermogravimetric analysis (TGA) in N_2 atmosphere.

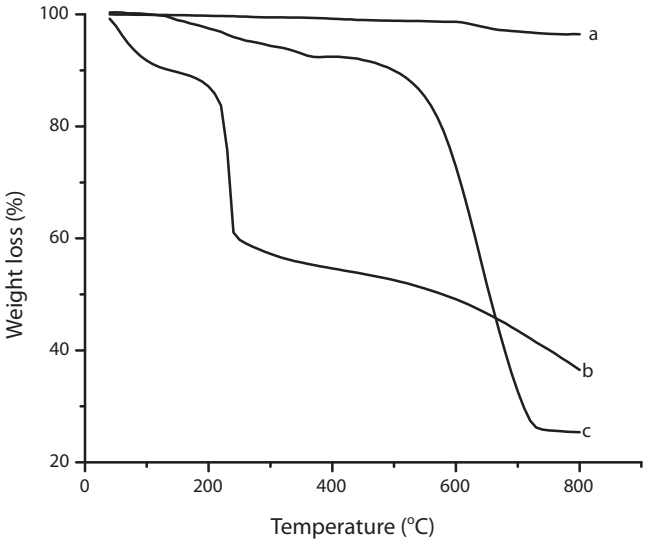

Figure 1. TGA curves of a) pencil, b) GO, and c) GNs.

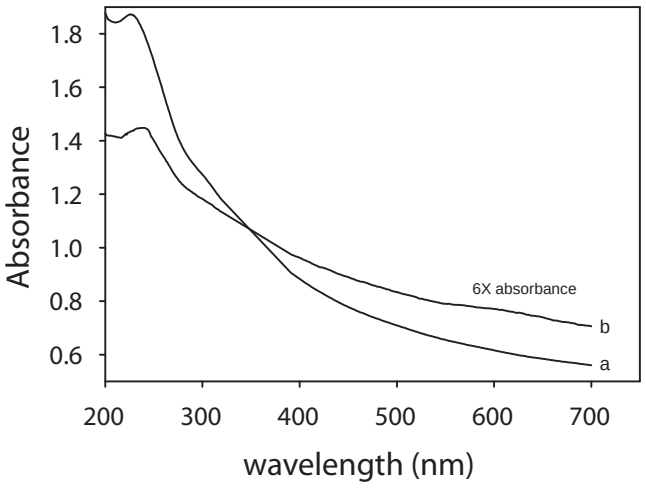

Figure 2. UV-vis spectrum of a) GO dispersed in water and b) GNs in water.

The TGA curves of the pencil, GO, and GNs are shown in **Figure 1**. As shown in Figure 1a, the pencil starts to lose weight at 650 °C due to combustion to carbon dioxide. Three significant weight loss events were observed for GO (Figure 1b), corresponding to the evaporation of water (below 100 °C) as GO adsorbs water under ambient conditions and readily desorbs water upon heating. The other two weight losses occurred at 120–150 °C and 220–250 °C due to the loss of carbon oxide gas species from labile oxygen containing groups, illustrating a lower thermal stability because of more functional groups in GO.[39,40] The TGA curve of the GNs (Figure 1c) exhibited two step of mass loss, one at 170 °C due to loss of carbon oxide gas species and another at an onset temperature of 550 °C, it may be due to the carbon oxidation and this TGA plot is same as reported earlier.[41] The above results indicate that almost no water molecules are trapped in GNs; this confirms the hydrophobicity of the GNs material. It is important to mention here that both GO and GNs were subjected to dialysis for three days. Hence, no mass loss for IL is observed in the GO and GNs when compared to other studies[42,43] in which dialysis was not conducted. Moreover, the complete removal of IL from GO and GNs is also confirmed by Fourier transform infrared (FTIR) spectroscopy and energy-dispersive spectrometry (EDS) in this work (see Supporting Information).

UV-vis absorption spectroscopy was also used to gain further insight into the quality of in situ electrochemically prepared GO and GNs. **Figure 2**a,b shows the UV-vis spectrum of GO and GNs suspension in water, respectively. The UV-vis spectra of GO exhibit an maximum absorption peak at about 228 nm, corresponding to $\pi \rightarrow \pi^*$ transition of aromatic C=C bonds and another at 300 nm due to $n \rightarrow \pi^*$ transitions of the carbonyl groups.[44,45] On the other hand, GNs (Figure 2b) exhibits a peak approximately at 250 nm, a typical $\pi \rightarrow \pi^*$ transition for the aromatic C=C bond in graphene and the typical absorption at 550 nm corresponding to the monolayer nature of graphene as shown in Figure 2b, which is absent in GO spectra.[44–48] This phenomenon of red shift (GO 228 nm to GNs 250 nm) was previously reported when GO was reduced[48] to GNs and used as a monitoring tool for the presence of GNs.[44]

Raman spectroscopy was used to know about the quality of the IL grown GO and GNs. Raman spectra in **Figure 3** reflect the significant structural changes that occurred during the electrochemical processing from pencil to GO and GNs. Moreover, the Raman spectrum of the pencil (Figure 3a) displays a prominent G peak at 1583 cm^{-1} corresponding to the first-order scattering of the E_{2g} vibration mode and a D band at 1311 cm^{-1} arising from a breathing mode of k-point phonons of A_{1g} symmetry.[49,50] Figure 3b shows the Raman spectrum of GO; the G band is broadened and the D band shifted to 1352 cm^{-1} and becomes prominent, showing an increased D/G intensity ratio of 0.75 indicating the distortion of bonds and destruction of symmetry probably due to the reduction in size of the in-plane sp^2 domains caused by the oxidation.[49,50] The intensity ratio of the D and G band is a measure of the disorder, as expressed by the sp^3/sp^2 carbon ratio.[51] Moreover, the vibration frequency of the G band increased to 1594 cm^{-1}, slightly higher than that in pencil, which can be attributed to the influence of defects and isolated double bonds.[52] It is noteworthy to explain here, usually the GNs synthesized by chemical approach show a strong D band in the Raman spectrum due to defects and partially disordered crystal structure of GNs. However, it is observed here that the intensity of G band (Figure 3c) is significantly higher than that of D band for the GNs obtained, suggesting that the prepared GNs have low defect content when compared to other reports.[53,54] The intensity of the 2D peak at 2657 cm^{-1} in GNs is greater when compared to pencil and GO and this is attributed to monolayer GNs, as reported earlier.[55]

The detailed morphology and crystalline structure of electrochemically prepared GNs were also studied by scanning electron microscopy (SEM), atomic force microscopy (AFM), transmission electron microscopy (TEM), high-resolution transmission electron microscopy (HRTEM), selected area electron diffraction (SAED), and X-ray diffraction (XRD) study. **Figure 4**a–c shows the SEM images of pencil, GO, and GNs, respectively. SEM image of GO (Figure 4b) is composed of fluffy and aggregates of crumpled sheets of GO as reported

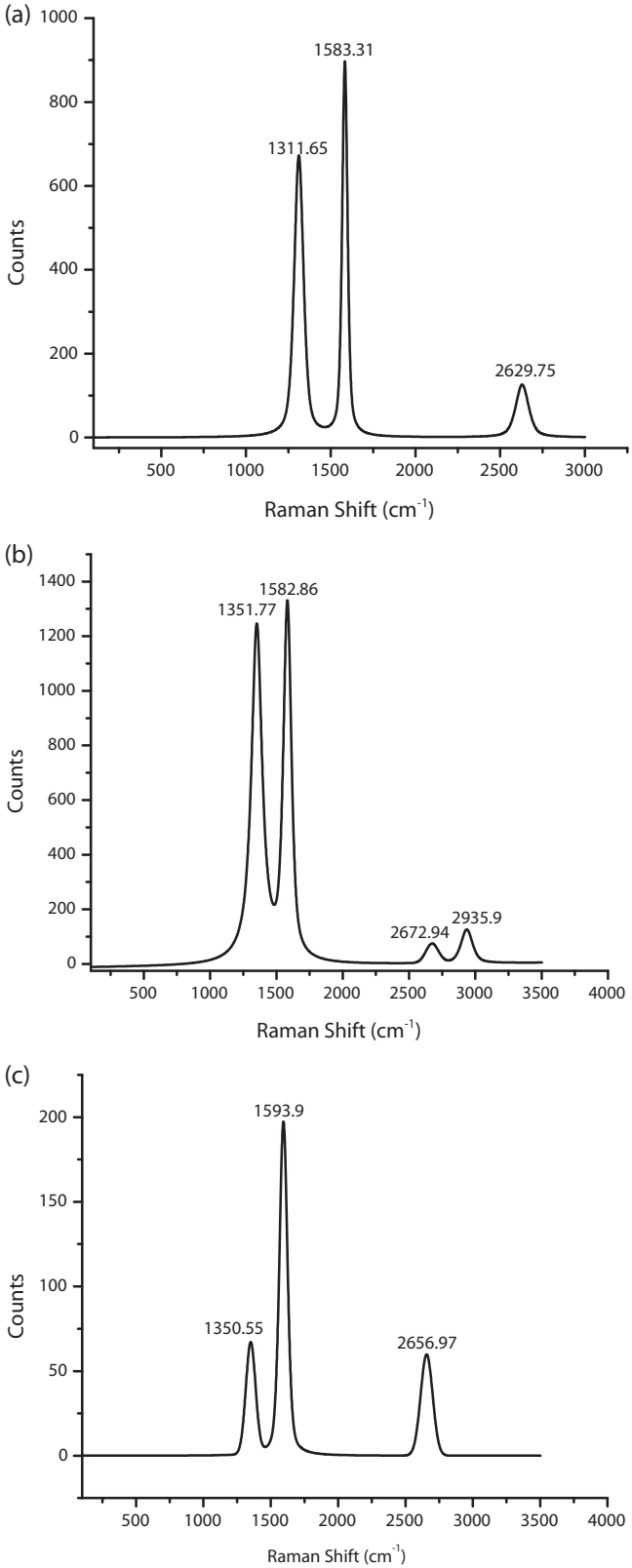

Figure 3. Raman spectrum of a) pencil, b) GO, and c) GNs.

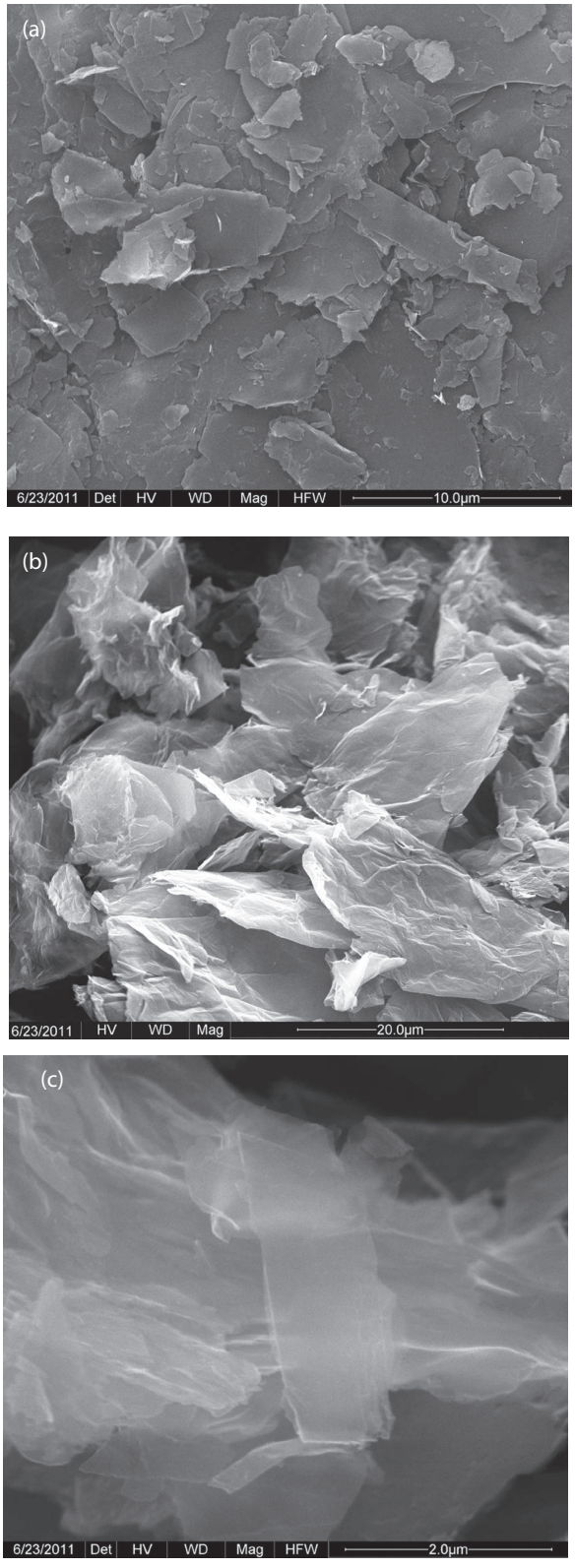

Figure 4. SEM images of a) pencil, b) GO, and c) GNs.

previously.[38] Figure 4c shows a SEM image of GNs, showing a transparent sheet-like structure and one can easily see the thin sheets of GNs in this image. The synthesized GNs appear transparent under the electron microscope, indicating that the morphological features of the electrochemically prepared GNs are similar to those GNs prepared by other approaches. The

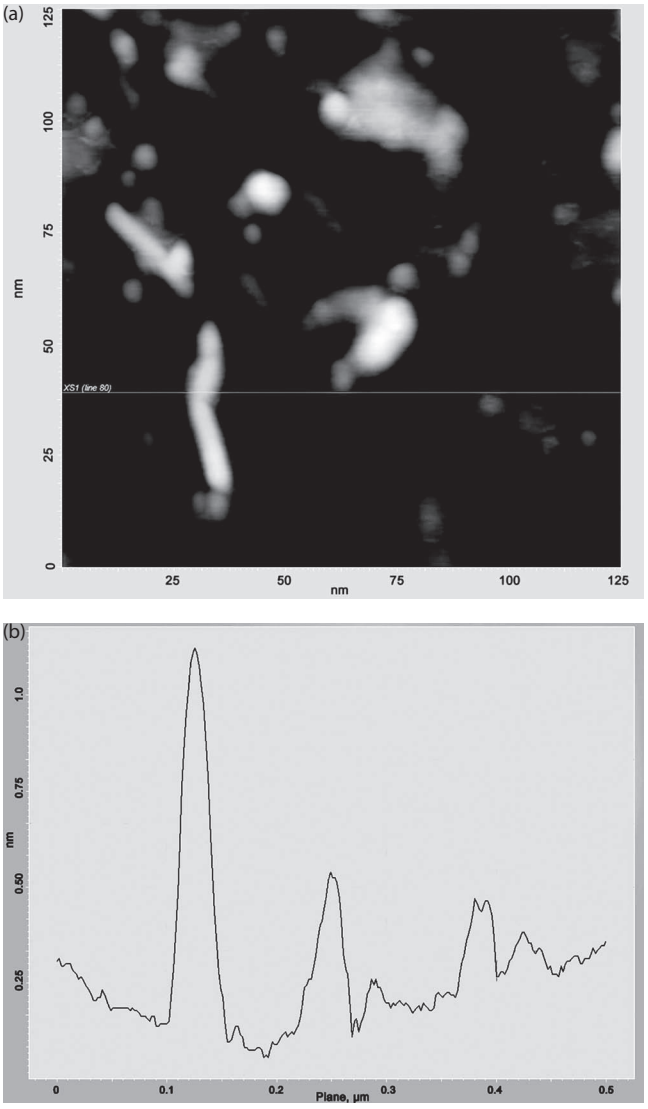

Figure 5. Semicontact AFM images of GNs on mica. a) Topographic view of the few large size and small size GNs and b) height profile through the line shown in (a).

absence of charging during the SEM imaging indicates that the network of GNs and the individual graphene sheet are electrically conductive.

The thickness and morphology of the GNs were further probed using AFM. **Figure 5** shows the AFM image and the cross sectional profile of generated GNs deposited on freshly cleaved mica surface. The AFM images reveal the presence of irregularly shaped sheets of non-uniform thickness and their lateral dimension ranging to a few nanometers. The sheet marked by the line in Figure 5a exhibited thicknesses between 0.8 and 1.3 nm, which is assigned to single-layer graphene sheets by the corresponding height profile diagram (Figure 5b) of the AFM image as reported earlier.[56,57] The above result confirms the achievement of electrochemical exfoliation of pencil to individual GNs under these experimental conditions in neat IL.

Figure 6a shows a low magnification TEM image of GNs. GNs are rippled and entangled with each other. They are transparent and very stable under the electron beam. The most transparent and featureless regions indicated by arrows in Figure 6a are probably due to the monolayer of GNs.[52] We also observed scrolled GNs (Figure 6a) as reported previously.[58] This is because the thermodynamic stability of the 2D GNs results from microscopic crumpling via bending or buckling. Figure 6b shows a high-magnification TEM image of GNs. The ordered graphite lattices are clearly visible. The SAED was also performed for the GNs and the corresponding SAED pattern is shown as the inset in Figure 6b and well-defined diffraction spots pattern in a ring are observed, which confirms the hexagonal graphitic structure for the crystalline nature of the GNs. The morphology and structure of the GO was also observed by TEM analysis. Figure 6c shows a TEM image of GO, clearly illustrating the flake-like shapes of GO. SAED pattern (inset in Figure 6c) further confirmed the disordered nature of the GO. The SAED pattern of GO shows only diffraction rings and the diffraction dots are unresolved, unambiguously indicating that the GO is amorphous. We also found that the GO was unstable under electron beam bombardment. After a few minutes of exposure to the electron beam during the TEM observation, the GO was found to be broken and this may be caused by the evaporation of the oxygen and hydrogen containing functionalized groups.[54]

The crystal structure of the pencil, GO and GNs are analyzed by conducting X-ray diffraction (XRD) studies. **Figure 7** shows the XRD data for pencil, GO, and GNs. The pencil exhibits a sharp peak centered at 26.6° (Figure 7a) corresponding to the (002) interplanar spacing of 3.36 Å. A shift in the (002) Bragg reflection from 26.6° to 11.66° is observed in GO (Figure 7b) and this reveals the successful exfoliation of pencil and is in good agreement with the reported value.[59] The disappearance of the GO peak at 11.66° due to the reduction process indicates removal of oxygen functionalities in GNs (Figure 7c). The GNs shows the peak broadening (Figure 7c) and shift in the 002 Bragg reflections towards lower angle when compared to pencil. The broader peak may be due to the corrugated structure of the GNs.[60,61] Therefore, the XRD, HRTEM, and SAED analyses clearly demonstrate that the electrochemical exfoliation of pencil using neat IL possesses fewer defects when compared to chemical methods reported so far.[53,54] Moreover, the XRD, HRTEM, and SAED analyses also clearly indicate that electrochemical synthesis are able to produce crystalline 2D GNs. The Supporting Information includes FTIR, EDS, and BET (Brunauer, Emmet, and Teller) surface area data for GNs (Figure S1, S2, and S3).

GO is an ideal material for the preparation of biosensors owing to the novel properties such as specific surface area, good biocompatibility, and physiological stability.[62,63] Hence, a bare SPR gold chip was modified with an ethanolic solution of GO containing 3-mercaptopropyl trimethoxy silane (MPTS) using a spin coater. In order to get uniform coating of GO on the SPR gold chip, the GO solution was made with MPTS in ethanolic medium[64,65] and then 75 µL of this solution was dispensed on bare SPR gold chip at 100 rpm. After this, spin speed was increased up to 2500 rpm and kept for 5 min to spread the liquid homogeneously on the SPR gold chip. As a result of adsorption of GO on SPR gold chip, the SPR angle was shifted

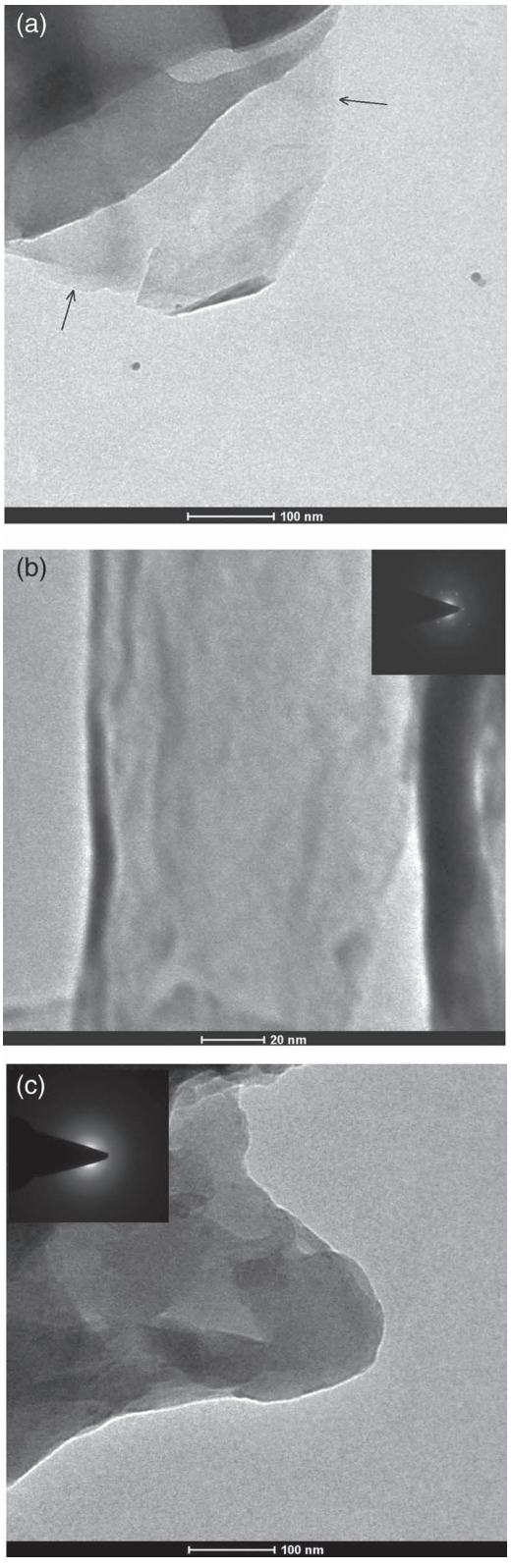

Figure 6. TEM images. a) Low-magnification TEM image of GNs, resembling crumpled silk. The featureless regions indicated by the arrows are monolayer GNs, b) HRTEM image of GNs. The inset is the SAED, which confirms the crystalline nature of the GNs, and c) TEM image of GO. The inset shows the corresponding SAED pattern.

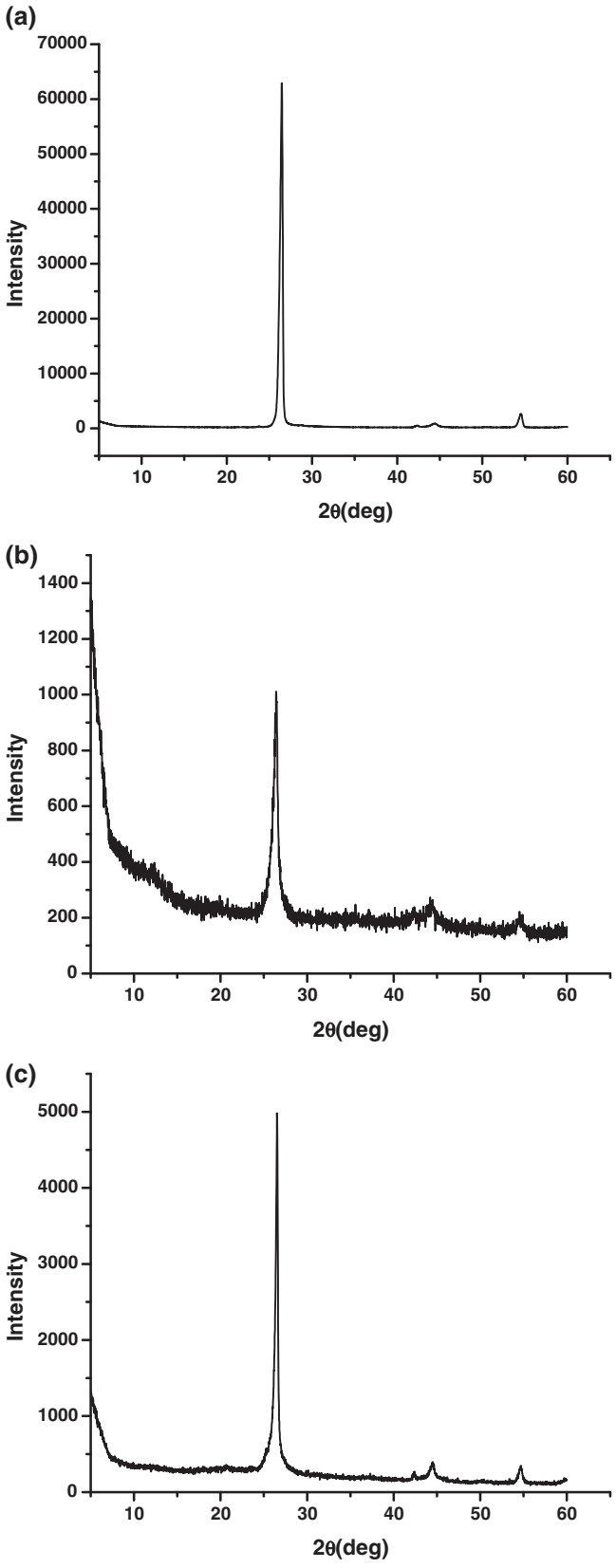

Figure 7. XRD pattern of a) pencil, b) GO, and c) GNs.

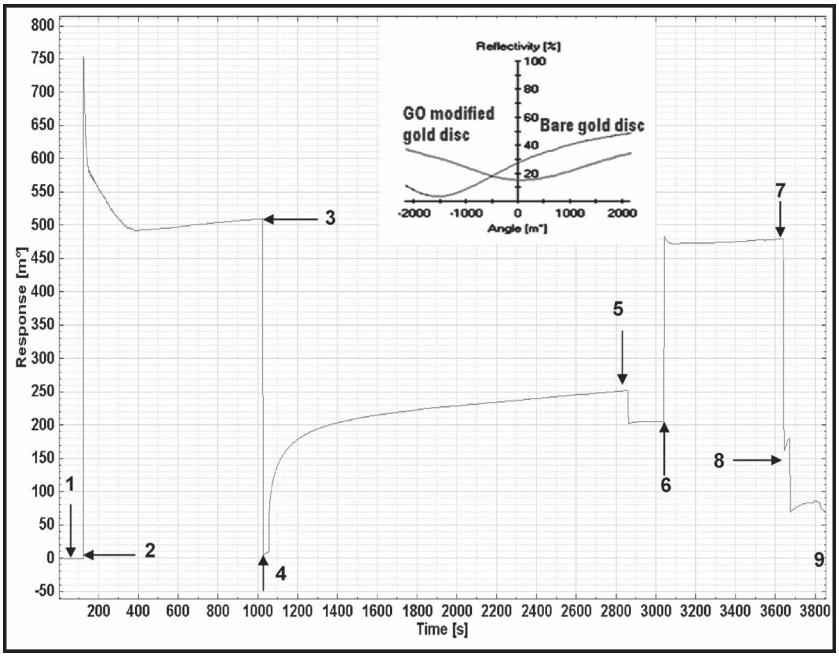

Figure 8. Sensorgram showing different steps: 1) baseline, 2) EDC-NHS activation, 3) washing, 4) Ag coupling, 5) washing, 6) deactivation, 7) washing, 8) regeneration, and 9) return to baseline, all of which are involved in the immobilization of *S. typhi* Ag on the GO-modified SPR gold chip.The inset shows the SPR angle shift after immobilization of GO on bare SPR gold chip.

from –1500 m° to 0 m° (inset of **Figure 8**); this confirms the modification of SPR gold chip with GO. GO has multifunctional groups including –COOH, which helps with the implementation of *N*-(3-dimethylaminopropyl)-*N*-ethylcarbodiimide hydrochloride (EDC)–*N*-hydroxysuccinimide (NHS) chemistry for the immobilization of protein molecules on the SPR gold chip (**Scheme 2**).

Figure 8 shows the stepwise immobilization of *S. typhi* Ag on a GO-modified SPR gold chip (see Experimental Section) and this process is composed of nine steps. Figure 8, in the first step, stabilization of baseline was carried out for 120 s. In second step, activation of carboxyl groups on a GO-modified SPR gold chip was performed for 900 s with EDC-NHS to enable activated carboxyl groups on the SPR gold chip to bind covalently to the free amino groups of *S. typhi* Ag upon its interaction. In third step, washing was conducted with phosphate buffer saline (PBS) and the SPR angle shifted nearly to baseline.[66] In fourth step, *S. typhi* Ag was injected on the GO-modified SPR gold chip, allowed it to interact for 1800 s and an increase in the SPR angle is observed. In fifth step, washing was performed and in sixth step, to prevent non-specific binding and also for the blocking of unreacted NHS ester groups on the GO-modified SPR gold chip, 1000 mM ethanolamine was used and allowed to react with sensor surface for 600 s. In seventh step, washing was performed for 30 s. In eighth step, regeneration was carried out for 120 s. At last in the ninth step, a back to base line process was conducted for 60 s. From Figure 8, a net angle change of 70.05 m° is observed and this indicates the attachment of 0.58 ng mm^{-2} of *S. typhi* Ag on a GO-modified SPR gold chip.[67]

The *S. typhi* Ag-immobilized, GO-modified SPR gold chip was used for the sensing of *S. typhi* Mab by interacting with different concentration of the *S. typhi* Mab and the results are depicted as a SPR sensorgram in **Figure 9**. The sensorgram in Figure 9 exhibits concentration-dependent angle changes, upon the interaction of various dilution of *S. typhi* Mab with its immobilized *S. typhi* Ag. A calibration graph (**Figure 10**) was constructed using the logarithm data of the angle change (Figure 9) against dilution of S. *typhi* Mab. This exhibited a linearity over the dilution range from 1:25 600 to 1:100 with correlation coefficient (r^2) value of 0.98. This shows the usability of GO in SPR sensing applications.

In order to find out the effect of temperature on SPR measurements during the binding of *S. typhi* Mab with immobilized *S. typhi* Ag, a temperature variation study was carried out between 10 and 37 °C with a 3 °C increment. A pH variation study was also conducted using acetate buffer (pH 4.0–5.5), phosphate buffered saline (pH 6.0–7.5), and glycine-NaOH buffer (pH 8.0–9.0) so as to find the optimum pH for the binding of *S. typhi* Mab with immobilized *S. typhi* Ag. Upon increasing temperature from 10 to 25 °C, an increase in SPR angle is observed and beyond 25 °C, SPR angle decreased.[68] Hence, 25 °C was used as the optimum temperature for the interaction of *S. typhi* Mab with its immobilized *S. typhi* Ag (Figure S4a, Supporting Information). Figure S4b (Supporting Information) shows the effect of pH on the SPR angle due to the interaction of *S. typhi* Mab with its immobilized *S. typhi* Ag. It is observed from Figure S4b that the SPR angle increased with the increase in pH up to 7.5 and then decreased up to pH 9.0. This observation is probably due to the pH-dependent structural changes and electrostatic interactions on the GO-modified SPR gold chip between *S. typhi* Mab and *S. typhi* Ag, as reported previously.[69] All these observations suggest that in pH 7.5 PBS buffer, the *S. typhi* Ag and *S. typhi* Mab interaction is more effective and thereby results in more angle change, hence, pH 7.5 was preferred for further studies.

The reproducibility of the Ag-immobilized, GO-modified SPR gold chip was evaluated by making six *S. typhi* Ag-immobilized, GO-modified SPR gold chips independently on different days. They showed an acceptable reproducibility with a relative standard deviation (RSD) of 3.98%, indicating the good reproducibility of the resulting *S. typhi* Ag-immobilized, GO-modified SPR gold chip for practical applications. Moreover, storage stability for the *S. typhi* immobilized, GO-modified SPR gold chip was also investigated after storage in PBS (pH 7.4) at 4 °C for three months. Only a 10% decrease in sensitivity was obtained. The decreased sensitivity may be attributed to the decrease in *S. typhi* activity.

Electrochemical impedance spectroscopy (EIS) was also used to characterize the electron transfer properties of the GO-modified SPR gold chip. It is well known that in EIS the semicircle portion observed at higher frequency corresponds to the charge

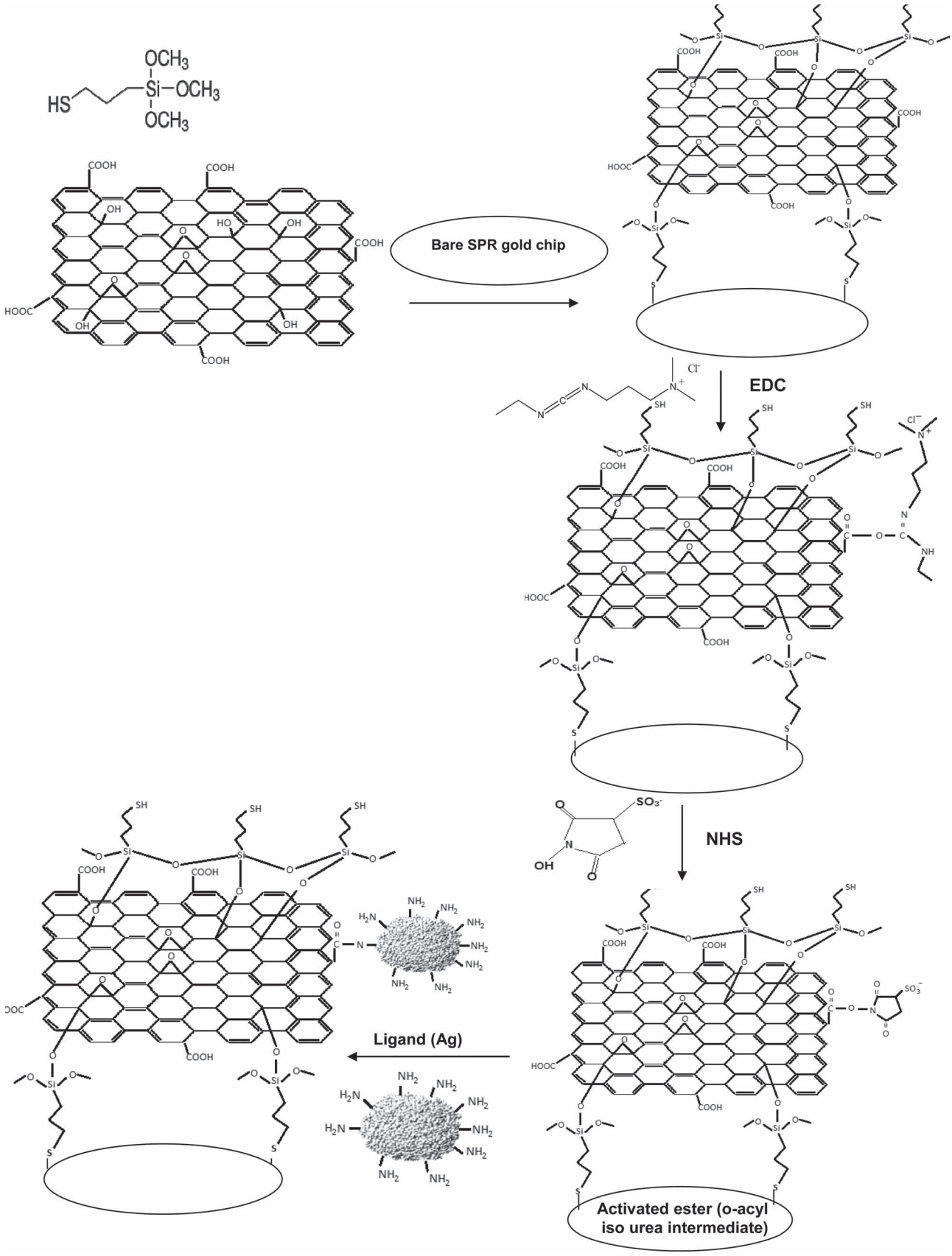

Scheme 2. Schematic representation of *S. typhi* Ag immobilization on a GO-modified SPR gold chip.

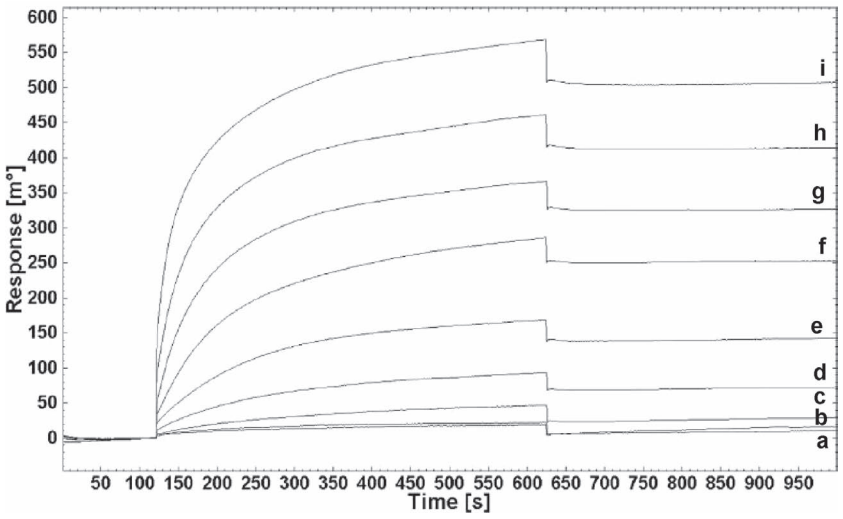

Figure 9. SPR sensor response for the interaction of different dilution of *S. typhi* Mab: a) 1:25 600; b) 1:12 800; c) 1:6400; d) 1:3200; e) 1:1600; f) 1:800; g) 1:400; h) 1:200; and i) 1:100 with immobilized *S. typhi* Ag. Temperature: 25 °C, pH: 7.5.

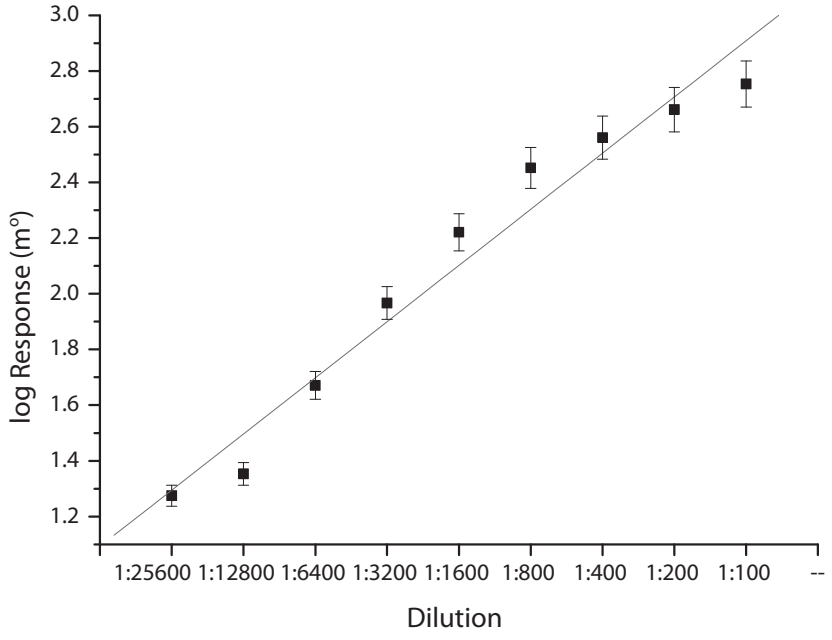

Figure 10. Calibration plot for the interaction of *S. typhi* Mab with immobilized *S. typhi* Ag. Temperature: 25 °C, pH: 7.5.

transfer limiting (R_{et}) process.[70] Figure S5a,b (Supporting Information) shows the Nyquist plot of the bare SPR gold chip and GO-modified SPR gold chip, respectively. After the modification of SPR gold chip with GO, the diameter of semicircle is increased compared to bare SPR gold chip and this is because of the inhibition of electron transfer due to the combined effect of MPTS and GO between solution and electrode interface. Hence, fit and simulation method was adopted to find out the R_{et} value for bare SPR gold chip and modified SPR gold chip with GO, the R_{et} values are found to be 501 kΩ and 641 kΩ, respectively.

3. Conclusions

A simple, greener, rapid, and cost-effective electrochemical method for the synthesis of GO and GNs from pencil is demonstrated at room temperature and subsequent potential use of GO for the modification of SPR gold chip in order to sense the BWA in label free and real time condition is achieved. The prepared GNs was characterized by SEM, TEM, AFM, XRD, UV-vis, and Raman spectroscopy and these confirmed the formation of single or double layer GNs with fewer defects (i.e., high quality). This methodology paves the way for using low purity carbon sources to grow high purity GO and GNs. Moreover, due to the simplicity of this method for the synthesis of GO and GNs, it may find promising applications in more areas in the development of many products.

4. Experimental Section

Materials: EDC, NHS, PBS, sodium acetate, ethanolamine, and hydrochloric acid (HCl) were obtained from Fluka and used as received, unless otherwise mentioned. IL [triethyl sulfonium bis (trifluromethyl sulfonyl) imide], glacial acetic acid, glycine, carbon tetrachloride, MPTS, and NaOH were supplied by Sigma-Aldrich. All chemicals and reagents used were of analytical grade and purification was performed wherever necessary before use. Pencil (9B) was used. BWA *S. typhi* Ag was isolated and also *S. typhi* Mab was raised by trained biologists in our establishment with appropriate protective measures. GO-modified SPR gold chip was used for SPR measurements. Different buffer solutions were used in this study depending on pH (acetate buffer (pH 4.0–5.5), PBS (pH 6.0–7.5), and glycine-NaOH buffer (pH 8.0–9.0)) for the optimization of pH. All solutions were prepared using water from a Milli-Q system throughout the experiment.

Synthesis of GO and GNs: In a typical electrochemical synthesis of GNs, a conventional three-electrode system was used, which consisted of pencil as a working electrode, Pt as a quasi-reference electrode, and Pt spiral as a counter electrode in IL electrolyte (10 mL). Static potentials of +0 V (120 s), +8 V (600 s), and –8 V (600 s) were applied. After 25 min, the pencil was exfoliated and then a black precipitate gradually appeared at the bottom of the electrochemical cell. The as-generated GNs were separated from the reaction mixture through decantation of IL; this IL could be reused for further GNs synthesis after distillation. The remaining dispersion was centrifuged at low speed (2000 rpm) to remove large agglomerates with CCl_4 and water as this IL dissolved in organic solvents only. The top of dispersion was then decanted and the bottom black precipitate of GNs was taken out of the vessel, thoroughly washed with Milli-Q water followed by ethanol, and then finally it was purified by dialysis for 3 days to remove the remaining impurities and then the resulting solid was finally dried at 80 °C. Many different potentials were selected for the electrochemical exfoliation of pencil in IL and the experimental results are given as Table S1 (Supporting Information).

Immobilization of S. typhi Ag on GO-Modified SPR Gold Chip: Prior to the immobilization of *S. typhi* Ag on the GO-modified SPR gold chip, PBS buffer (50 µL, pH 7.5) was passed every 120 s interval for 600 s in order to obtain a stable baseline in both channels. The GO-modified SPR gold chip was chemically activated by the injection of a 1:1 mixture of 400 mM EDC (50 µL) and 100 mM NHS (50 µL). Subsequently, *S. typhi* Ag (50 µL, 1:500 dilution in 10 mM PBS) was injected in channel 2 for 1800 s to obtain an effective immobilization of *S. typhi* Ag on the activated GO-modified SPR gold chip surface. Following *S. typhi* Ag immobilization, the remaining active sites were then blocked with of 1000 mM ethanolamine (50 µL). Afterwards, HCl (10 mM) was injected to achieve regeneration of immobilized SPR gold chip. For negative control measurements, the modified SPR gold chip was activated with EDC-NHS and then quenched with ethanolamine in channel 1 as mentioned above and was used as blank control surface.

Biosensing Protocol: For the kinetic measurements of *S. typhi* Mab, different dilutions of *S. typhi* Mab were prepared in PBS. The entire SPR sensing methodology was executed by a sequence of automatic procedure (baseline, association, dissociation, regeneration, and back to baseline steps). A sample solution containing a selected concentration of *S. typhi* Mab in the PBS was injected in both channels from the 384-well microtiter plate and then association was performed for 500 s and dissociation was performed for 400 s. Subsequently, regeneration of the sensor surface was achieved by addition of HCl (10 mM) for 120 s. In the entire study, PBS (pH 7.5) was utilized as the running buffer solution. For SPR sensing, an aliquot of the analyte solution (35 µL) was injected and mixed at 16.5 µL s^{-1} and this protocol was followed from 1:25 600 to 1:100 dilution of *S. typhi* Mab.

Instruments: TEM was carried out with an FEI Technai G2 F20 microscope at 200 kV; the samples were air dried before using the TEM to characterize the size and morphology. For TEM observation, the samples were prepared in methanol (100 µg mL^{-1}) and dispersed in an ultrasonicator for 10 min. The samples for TEM analysis were obtained by placing a drop of the colloidal dispersion onto the 200 mesh carbon-coated copper grid. They were dried at room temperature and then examined using the TEM without any further modification. The crystal structure of samples was studied using a Bruker D8 Advance X-ray Diffractometer operating at 40 mA and 40 kV, Cu Kα 1 monochromatic radiation. The surface morphology of the samples was studied using atomic force microscope (NT-MDT: NTEGRA Model) in semicontact mode with special emphasis on sheet thickness, morphological features, and lateral dimensions. Samples of GNs were prepared as suspension in dimethylformamide (DMF). The suspension was ultrasonicated for 30 min. This suspension was diluted to a concentration of 0.02 mg mL^{-1}. TGA was used to investigate the thermal behaviors of the pencil, GO, and GNs. Thermogram of pencil, GO, and GNs were recorded using TGA-2950 from TA instruments (USA) under N_2 atmosphere. Electrochemical studies were performed with a potentiostat/galvanostat with frequency response analyzer (Autolab-302N with FRA, The Netherlands). Morphology and elemental composition of the samples were studied by SEM-EDS (Quanta400-ESEM, The Netherlands). Raman spectra were obtained using Renishaw Invia Raman Microscope (Gloucestershire, UK) to identify the functional groups. FTIR spectroscopy studies were performed using an IR spectrometer Perkin Elmer, Inc.; Shelton, CT, USA with a KBr pellet.

A conventional three-electrode system used here consisted of pencil as the working electrode, Pt as the quasireference electrode, and Pt spiral as the counter electrode of Metrohm make. The biomolecular interactions were conducted using a two-channel, cuvette-based electrochemical SPR (ESPR) system (Autolab ESPRIT, Ecochemie B.V.; The Netherlands). The outcome of the SPR measurement was monitored using a PC with data acquisition using the SPR software version 4.3.1. Electrochemical studies were performed in the ESPR cuvette cell coupled to a three-electrode system. The SPR gold chip was the working electrode, Ag/AgCl was the reference electrode, and Pt was the counter electrode. For EIS studies, a FRA II module with FRA software 4.9 (Ecochemie B.V., The Netherlands) was used. The pH of the buffers was measured with a EUTECH instrument pH meter (pH-1500, Singapore). All SPR and EIS experiments were carried out at 25 °C unless otherwise specified and the temperature of cuvette was controlled by a Julabo HE-4 (Germany) water bath.

Supporting Information

Supporting Information is available from the Wiley Online Library or from the author.

Acknowledgements

The authors thank Prof. Dr. M. P. Kaushik, Director, Defence Research and Development Establishment, DRDO, Gwalior-474002 (India) for his keen interest and encouragement.

Received: October 20, 2011
Revised: January 28, 2012
Published online: March 13, 2012

[1] K. S. Novoselov, A. K. Geim, S. V. Morozov, D. Jiang, Y. Zhang, S. V. Dubonos, I. V. Grigorieva, A. A. Firsov, *Science* **2004**, *306*, 666.
[2] K. I. Bolotin, K. J. Sikes, Z. Jiang, M. Klima, G. Fudenberg, J. Hone, P. Kim, H. L. Stormer, *Solid State Commun.* **2008**, *146*, 351.
[3] B. F. Machado, P. Serp, *Catal. Sci. Technol.* **2012**, *2*, 54.
[4] K. S. Novoselov, D. Jiang, F. Schedin, T. J. Booth, V. V. Khotkevich, S. V. Morozov, A. K. Geim, *Proc. Natl. Acad. Sci. USA* **2005**, *102*, 10451.
[5] K. S. Novoselov, A. K. Geim, S. V. Morozov, D. Jiang, M. I. Katsnelson, I. V. Grigorieva, *Nature* **2005**, *438*, 197.
[6] A. Reina, X. Jia, J. Ho, D. Nezich, H. Son, V. Bulovic, M. S. Dresselhaus, J. Kong, *Nano Lett.* **2009**, *9*, 30.
[7] Y. Hernandez, V. Nicolosi, M. Lotya, F. M. Blighe, Z. Sun, S. De, I. T. McGovern, B. Holland, M. Byrne, Y. K. Gunoko, J. J. Boland, P. Niraj, G. Duesberg, S. Krishnamurthy, R. Goodhue, J. Hutchison, V. Scardaci, A. C. Ferrari, J. N. Coleman, *Nat. Nanotechnol.* **2008**, *3*, 563.
[8] G. M. Rutter, J. N. Crain, N. P. Guisinger, T. Li, P. N. First, J. A. Stroscio, *Science* **2007**, *317*, 219.
[9] C. Zhu, S. Guo, Y. Fang, S. Dong, *ACS Nano* **2010**, *4*, 2429.
[10] D. Luo, G. Zhang, J. Liu, X. Sun, *J. Phys. Chem. C* **2011**, *115*, 11327.
[11] C. Y. Su, A. Y. Lu, Y. Xu, F. R. Chen, A. N. Khlobystov, L. J. Li, *ACS Nano* **2011**, *5*, 2332.
[12] S. Park, R. S. Ruoff, *Nat. Nanotechnol.* **2009**, *4*, 217.
[13] S. Park, J. An, I. Jung, R. D. Piner, S. J. An, X. Li, A. Velamakanni, R. S. Ruoff, *Nano Lett.* **2009**, *9*, 1593.
[14] C. Gomez-Navarro, R. T. Weitz, A. M. Bittner, M. Scolari, A. Mews, M. Burghard, K. Kern, *Nano Lett.* **2009**, *9*, 2206.
[15] A. A. Green, M. C. Hersam, *Nano Lett.* **2009**, *9*, 4031.
[16] S. J. Park, R. S. Ruoff, *Nat. Nanotechnol.* **2009**, *4*, 217.
[17] A. Zhamu, B. Z. Zhang, *US Patent* 20090028778, **2009**.
[18] S. Vadukumpully, J. Paul, S. Valiyaveettil, *Carbon* **2009**, *47*, 3288.
[19] X. Li, H. Wang, J. T. Robinson, H. Sanchez, G. Diankov, H. Dai, *J. Am. Chem. Soc.* **2009**, *131*, 15939.
[20] D. W. Boukhvalov, M. I. Katsnelson, *J. Am. Chem. Soc.* **2008**, *130*, 10697.
[21] H. L. Guo, X. F. Wang, Q. Y. Qian, F. B. Wang, X. H. Xia, *ACS Nano* **2009**, *3*, 2653.
[22] X. Fan, W. Peng, Y. Li, X. Li, S. Wang, G. Zhang, *Adv. Mater.* **2009**, *20*, 4490.
[23] J. G. Huddleston, R. D. Rogers, *Chem. Commun.* **1998**, *16*, 1765.
[24] G. A. Snook, A. S. Best, *J. Mater. Chem.* **2009**, *19*, 4248.

[25] A. Safavi, N. Maleki, F. Tajabadi, E. Farjami, *Electrochem. Commun.* **2007**, *9*, 1963.
[26] J. M. Pringle, O. Ngamna, C. Lynam, G. G. Wallace, M. Forsyth, D. R. MacFarlane, *Macromolecules* **2007**, *40*, 2702.
[27] F. Xiao, F. Zhao, J. Li, L. Liu, B. Zeng, *Electrochim. Acta* **2008**, *53*, 7781.
[28] C. L. Lin, C. H. Chiu, C. Chu, Y. C. Huang, T. Y. Lin, J. T. Ou, *J. Microbiol. Immunol. Infect.* **2007**, *40*, 222.
[29] P. T. Feldsine, A. H. Lienau, S. C. Leung, L. A. Mui, F. Humbert, M. Bohnert, K. Mooijman, S. Schulten, P. Veld, P. Rollier, R. Leuschner, K. J. Capps, *AOAC Int.* **2003**, *86*, 275.
[30] S. Kumar, K. Balakrishna, H. Batra, *Biomed. Environ. Sci.* **2008**, *21*, 137.
[31] C. G. De Freitas, A. P. Santana, P. H. C. da Silva, V. S. P. Goncalves, M. A. F. Barros, F. A. G. Torres, L. S. Murata, S. Perecmanis, *Int. J. Food Microbiol.* **2010**, *139*, 15.
[32] C. F. Pui, W. C. Wong, L. C. Chai, E. Nillian, F. M. Ghazali, Y. K. Cheah, Y. Nakaguchi, M. Nishibuchi, S. Radu, *Food Control* **2011**, *22*, 337.
[33] G. F. I. Widal, A. Sicard, *Bull. Soc. Med. Paris* **1896**, *13*, 682.
[34] G. Gupta, P. K. Singh, M. Boopathi, D. V. Kamboj, B. Singh, R. Vijayaraghavan, *Thin Solid Films* **2010**, *519*, 1171.
[35] G. Gupta, A. S. B. Bhaskar, B. K. Tripathi, P. Pandey, M. Boopathi, P. V. L. Rao, B. Singh, R. Vijayaraghavan, *Biosens. Bioelectron.* **2011**, *26*, 2534.
[36] F. Kang, Y. Leng, T. Y. Zhang, *J. Phys. Chem. Solids* **1996**, *57*, 889.
[37] R. A. Greinke, R. A. Reyolds, *US Patent* 6416815, **2002**.
[38] D. Du, L. Wang, Y. Shao, J. Wang, M. H. Engelhard, Y. Lin, *Anal. Chem.* **2011**, *83*, 746.
[39] S. Stankovich, D. A. Dikin, R. D. Piner, K. A. Kohlhaas, A. Kleinhammes, Y. Jia, Y. Wu, S. T. Nguyen, R. S. Ruoff, *Carbon* **2007**, *45*, 1558.
[40] H. K. Jeong, M. H. Jin, K. P. So, S. C. Lim, Y. H. Lee, *J. Phys. Appl. Phys.* **2009**, *42*, 0654181.
[41] G. Wang, J. Yang, J. Park, X. Gou, B. Wang, H. Liu, J. Yao, *J. Phys. Chem. C* **2008**, *112*, 8192.
[42] N. Liu, F. Luo, H. Wu, Y. Liu, C. Zhang, J. Chen, *Adv. Funct. Mater.* **2008**, *18*, 1518.
[43] T. Y. Kim, H. W. Lee, J. E. Kim, K. S. Suh, *ACS Nano* **2010**, *4*, 1612.
[44] D. Li, M. B. Muller, S. Gilje, R. B. Kaner, G. G. Wallace, *Nat. Nanotechnol.* **2008**, *3*, 101.
[45] M. Feng, H. Zhan, Y. Chen, *Appl. Phys. Lett.* **2010**, *96*, 033107.
[46] R. R. Nair, P. Blake, A. N. Grigorenko, K. S. Novoselov, T. J. Booth, T. Stauber, N. M. Peres, A. K. Geim, *Science* **2008**, *320*, 1308.
[47] Z. Sun, Z. Yan, J. Yao, E. Beitler, Y. Zhu, J. M. Tour, *Nature* **2010**, *468*, 549.
[48] T. Kim, H. Lee, J. Kim, K. S. Suh, *ACS Nano* **2010**, *4*, 1612.
[49] C. N. R. Rao, A. K. Sood, K. S. Subrahmanyam, A. Govindaraj, *Angew. Chem. Int. Ed.* **2009**, *48*, 7752.
[50] M. J. Allen, V. C. Tung, R. B. Kaner, *Chem. Rev.* **2010**, *110*, 132.
[51] A. C. Ferrari, J. Robertson, *J. Phys. Rev. B* **2000**, *61*, 14095.
[52] K. N. Kudin, B. Ozbas, H. C. Schniepp, R. K. Prudhomme, I. A. Aksay, R. Car, *Nano Lett.* **2008**, *8*, 36.
[53] L. Tang, Y. Wang, Y. Li, H. Feng, J. Lu, J. Li, *Adv. Funct. Mater.* **2009**, *19*, 2782.
[54] Z. Fan, Q. Zhao, T. Li, J. Yan, Y. Ren, J. Feng, T. Wei, *Carbon* **2012**, *50*, 1699.
[55] A. C. Ferrari, J. C. Meyer, V. Scardaci, C. Casiraghi, M. Lazzeri, F. Mauri, *Phys. Rev. Lett.* **2006**, *97*, 187401.
[56] J. I. Paredes, S. Villar-Rodil, A. Martinez-Alonso, J. M. D. Tascon, *Langmuir* **2008**, *24*, 10560.
[57] S. S. Li, K. H. Tu, C. C. Lin, C. W. Chen, M. Chhowalla, *ACS Nano* **2010**, *4*, 3169.
[58] J. C. Meyer, A. K. Geim, M. I. Katsnelson, K. S. Novoselov, T. J. Booth, S. Roth, *Nature* **2007**, *446*, 60.
[59] D. Cai, M. Song, *J. Mater. Chem.* **2007**, *17*, 3678.
[60] A. Celzard, J. F. Mareche, G. Furdin, *Prog. Mater. Sci.* **2005**, *50*, 93.
[61] S. Lee, D. Cho, L. T. Drzal, *J. Mater. Sci.* **2005**, *40*, 231.
[62] F. Qu, H. Lu, M. Yang, C. Deng, *Biosens. Bioelectron.* **2011**, *26*, 4810.
[63] L. M. Zhang, J. G. Xia, Q. H. Zhao, L. W. Liu, Z. J. Zhang, *Small* **2010**, *6*, 537.
[64] H. A. Becerril, J. Mao, Z. Liu, R. M. Stoltenberg, Z. Bao, Y. Chen, *ACS Nano* **2008**, *2*, 463.
[65] F. A. He, J. T. Fan, F. Song, L. M. Zhang, H. L. W. Chan, *Nanoscale* **2011**, *3*, 1182.
[66] W. C. Tsai, I. C. Li, *Sens. Actuators B: Chem.* **2009**, *136*, 8.
[67] E. Stenberg, B. Persson, H. Roos, C. Urbaniczky, *J. Colloid Interface Sci.* **1991**, *143*, 513.
[68] G. Gupta, P. K. Singh, M. Boopathi, D. V. Kamboj, B. Singh, R. Vijayaraghavan, *Thin Solid Films* **2010**, *519*, 1115.
[69] S. Paynter, D. A. Russell, *Anal. Biochem.* **2002**, *309*, 85.
[70] H. L. Guo, X. F. Wang, Q. Y. Qian, F. B. Wang, X. H. Xia, *ACS Nano* **2009**, *3*, 2653.